ELSEVIER

Journal of Fluids and Structures 26 (2010) 1078–1097

JOURNAL OF FLUIDS AND STRUCTURES

www.elsevier.com/locate/jfs

Investigation of turbulent flow past a yawed wavy cylinder

K. Lam[a,*], Y.F. Lin[a], L. Zou[b], Y. Liu[a]

[a]*Department of Mechanical Engineering, The Hong Kong Polytechnic University, Hung Hom, Kowloon, Hong Kong*
[b]*School of Mechanical and Electronic Engineering, Wuhan University of Technology, Wuhan 430070, China*

Received 22 September 2009; accepted 14 July 2010
Available online 16 September 2010

Abstract

A large eddy simulation (LES) study was conducted to investigate the three-dimensional characteristics of the turbulent flow past wavy cylinders with yaw angles from 0° to 60° at a subcritical Reynolds number of 3900. The relationships between force coefficients and vortex shedding frequency with yaw angles for both wavy cylinders and circular cylinders were investigated. Experimental measurements were also performed for the validation of the present LES results. Comparing with corresponding yawed circular cylinders at similar Reynolds number, significant differences in wake vortex patterns between wavy cylinder and circular cylinder were observed at small yaw angles. The difference in wake pattern becomes insignificant at large yaw angles. The mean drag coefficient and the Strouhal number obey the independence principle for circular cylinders at yaw angle less than 45°, while the independence principle was found to be unsuitable for yawed wavy cylinders. In general, the mean drag coefficients and the fluctuating lift coefficients of a yawed wavy cylinder are less than those of a corresponding yawed circular cylinder at the same flow condition. However, with the increase of the yaw angle, the advantageous effect of wavy cylinder on force and vibration control becomes insignificant.

Keywords: Large eddy simulation; Wavy cylinders; Yaw angle; Turbulent flow

1. Introduction

Flow past yawed or unyawed bluff bodies in widely encountered in engineering applications, such as cable suspension bridges, overhead cables, tow cables, chimney stacks, towers, offshore structures, etc. How to fully understand the complicated flow phenomena around a yawed cylindrical cable and how to reduced their bodies drag and fluctuating lift are important problems for engineering design. In fundamental research, flows past circular cylinders have been extensively investigated both experimentally and numerically. Many important physical phenomena were observed. For flow past yawed circular cylinders, Bursnall and Loftin (1951) experimentally investigated the pressure distribution of a yawed circular cylinder in the critical Reynolds number range. They showed that at critical Reynolds number, the flow and force characteristics of a yawed cylinder cannot be determined only by the component of flow normal to the axis of the cylinder when the yaw angle is greater than 45°. Hanson (1966) investigated the vortex shedding frequency of a yawed cylinder at low Reynolds number. Van Atta (1968) found that the Independence Principle (the drag coefficient

*Corresponding author.
E-mail address: mmklam@polyu.edu.hk (K. Lam).

0889-9746/$ - see front matter © 2010 Elsevier Ltd. All rights reserved.
doi:10.1016/j.jfluidstructs.2010.07.005

and the Strouhal number, which are normalized by the velocity component perpendicular to the cylinder, are approximately independent on the yaw angle of the circular cylinder) is true over a wide range of Reynolds number. The Independence Principle (also referred to as the cosine law) is not suitable for the determination of the Strouhal number for cylinders with a yaw angle greater than 60°. Ramberg (1983) experimentally investigated the vortex shedding characteristics on finite-length yawed cylinders. The foregoing researchers further confirmed that the Independence Principle was not suitable for a cylinder at large yaw angle. Further experimental investigations had been carried out by Shirakashi et al. (1984), Lourenco et al. (1992) and Hayashi and Kawamura (1995). Moreover, numerical simulations on yawed cylinders had also been carried out (Kawamura and Hayashi, 1994; Kaneko and Kawamura, 2002; Lucor and Karniadakis, 2003; Marshall, 2003; Thakur et al., 2004; Yeo and Jones, 2008; Vakil and Green, 2009; Zhao et al., 2009). Kaneko and Kawamura (2002) used direct numerical simulation (DNS) for flow past a yawed circular cylinder at subcritical Reynolds number of 1000 and found that the Independence Principle fails for the cylinder at large yaw angles. Thakur et al. (2004) showed same vortex shedding characteristics for yawed cylinder similar to that obtained by Van Atta (1968). Moreover, Vakil and Green (2009) numerical investigated yawed circular cylinders with finite aspect ratio with aspect ratios from 2 to 20D in the Reynolds number range from 1 to 40. Their results showed that the Independence Principle was not accurate for yaw angle larger than 45° in such flow conditions.

Aiming at the reduction of drag and the suppression of the fluctuating lift force on cylindrical structures, most of the experimental and numerical investigations had only been carried out on cross-flow around bluff bodies of unyawed cylinders as summarized by Choi et al. (2008). For example, Tombazis and Bearman (1997) introduced a spanwise wavy surface to the trailing face of the cylindrical bodies while Bearman and Owen (1998) and Dobre et al. (2006) investigated the effects of a spanwise wavy surface at the leading face of the cylindrical bodies. At Reynolds number 40 000, a maximum drag reduction of about 30% was obtained by Bearman and Owen (1998). Darekar and Sherwin (2001) numerically investigated the flow past a square cylinder with a wavy stagnation face at low Reynolds numbers. They showed that the unsteady and staggered Kármán vortex wake could be suppressed to a steady and symmetric wake structure due to the waviness of the square cylinder. A maximum drag reduction of about 16% was obtained at a Reynolds number of 100 compared with the straight, non-wavy square cylinder. At high Reynolds numbers, the drag reduction increases substantially. More recently, a special type of cylinder namely a wavy cylinder (a circular section cylinder with wavy variation of diameter along the spanwise direction) aiming at the reduction of vortex induced vibration was introduced by Lam et al. (2004). Lam and Lin (2007, 2008, 2009) carried out numerical simulations to study the flows around the wavy cylinders. The detailed three-dimensional wake structures behind the wavy cylinders were captured and the optimal values of spanwise wavelength λ/D_m base on the control of body's drag reduction were obtained. By using the large eddy simulation (LES) method, Lam and Lin (2008) found that a wavy cylinder with spanwise wavelength $\lambda/D_m = 1.9$ can lead to significant drag force reduction and vibration suppression at $\mathrm{Re} = 3000$. Moreover, Lam and Lin (2007, 2009) numerically investigated cross-flow past wavy cylinders with a wide range of spanwise wavelength in the low Reynolds number regime. Two optimal wavelengths for drag reduction were found at $\lambda/D_m = 2$ and $\lambda/D_m = 6$ for $\mathrm{Re} = 100$. With a larger value of spanwise wavelength $\lambda/D_m = 6$, the vortex shedding behind the wavy cylinder was greatly suppressed and the drag force was significantly reduced. Recently, Lam et al. (2010) carried out force measurements on a single wavy cylinder with wavelength ratio ($\lambda/D_m = 6$) at Re from 6800 to 13,400, and performed the large eddy simulation for the same wavy cylinder at $\mathrm{Re} = 7500$. The results showed that the mean drag coefficients of such wavy cylinder were evidently smaller than those of a purely circular cylinder within the same Reynolds number range. The fluctuating lift coefficients of the wavy cylinders are also smaller than that of a purely circular cylinder at the same Reynolds number. It was concluded that both the experimental and numerical results have confirmed that the wavy cylinder of $\lambda/D_m = 6$ was a suitable choice for the control of cylinder vibration and drag reduction.

Previous investigations have been concentrated on the study of different types of a single unyawed wavy cylinder in cross-flow ranging from low Reynolds numbers to subcritical Reynolds numbers. What happens to the vortex shedding phenomena and force coefficients for flows at different yaw angles of a wavy cylinder remain unanswered. Such study should give further insight to the understanding of the mechanism of force reduction by wavy cylinders at yawed conditions. Flows around yawed cylinders are quite common in engineering structures. It is hoped that this investigation will be helpful in industrial applications especially on the design of inclined cable-stayed bridges, tow cables, overhead cables, risers, etc. The present study investigates the flow around a wavy cylinder with different yaw angles. It aims at finding out whether this type of wavy cylindrical shape when used as inclined cables can suppress the body's fluctuating and reduce the drag force or not. It is anticipated that a detailed investigation could provide important information on the flow characteristics and hence be helpful to the designing of such engineering structures. By using large eddy simulation, the complex instantaneous three-dimensional (3-D) vortex structures can be captured. The vortex shedding characteristics, flow patterns and force characteristics of wavy cylinders at different yaw angles can

be obtained. The relationship between wavelength, yaw angle and force reduction can be fully investigated. Such study would also provide further understanding and discovery on the physical mechanisms of flow-induced vibration suppression, drag reduction and the 3-D wake vortices interactions of the wavy cylinders at different yawed angles. Considering the previous investigations discussed above, it is anticipated that the wavy cylinder with $\lambda/D_m = 6$ would give the best results on cylinder vibration suppression and drag reduction. As a result, a wavy cylinder with a spanwise wavelength ratio of $\lambda/D_m = 6$ and a wave amplitude of $a/D_m = 0.15$ was chosen in the present simulations, and five different yaw angles ($\alpha = 0$, 15, 30, 45 and 60°) of the cylinder were studied. Moreover, some typical cases were investigated by experimental measurements which can be used as supplements to the numerical results as well as for the validation of the numerical simulation.

2. Geometry of models

Fig. 1(a) shows the schematic diagram of a wavy cylinder ($\lambda/D_m = 6$, $a/D_m = 0.15$). The geometry can be described by

$$D_z = D_m + 2a\cos(2\pi z/\lambda), \tag{2.1}$$

and the mean diameter D_m is defined by

$$D_m = (D_{min} + D_{max})/2. \tag{2.2}$$

Here, D_z denotes the local diameter of the wavy cylinder and D_z varies sinusoidally in the spanwise z-direction. The amplitude of the wavy surface a is equal to half peak-to-peak distance. The spanwise wavelength λ is also indicated in Fig. 1(a). The axial location with maximum local diameter $D_{\max}$ is called a 'node', while the axial location with minimum diameter $D_{\min}$ is called 'saddle'. The diameter of the middle cross-section is also defined at mid-point between the node and the saddle. All geometrical lengths are normalized with the mean diameter D_m. Furthermore, a purely circular cylinder with diameter D_m is used for comparison purposes.

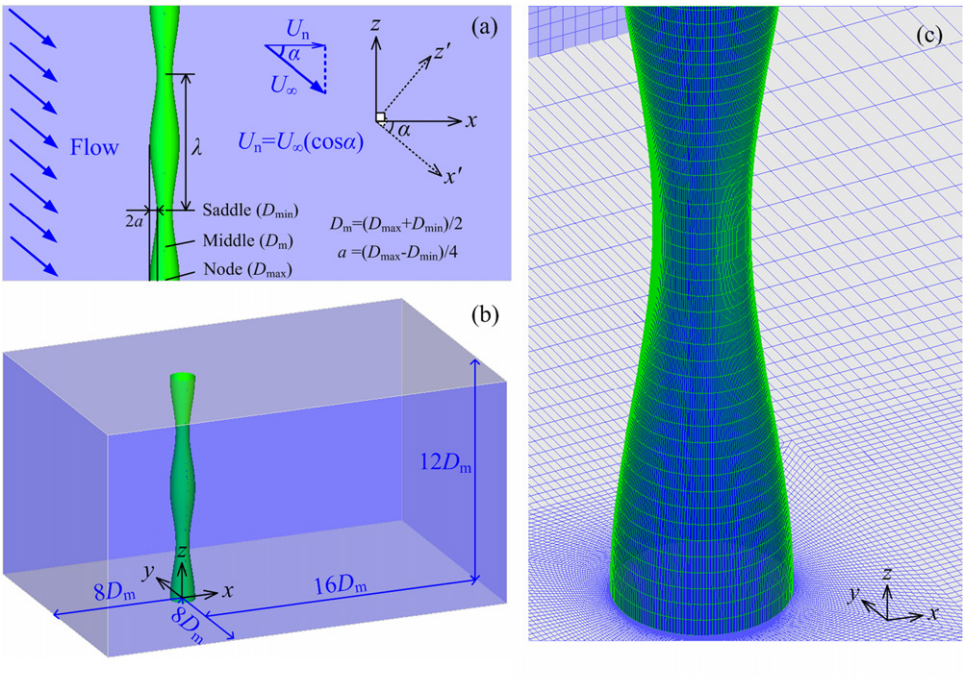

Fig. 1. Computational model: (a) geometry of a wavy cylinder, (b) schematic of the computational domain and (c) grid distributions around a wavy cylinder.

3. Computational method

3.1. Governing equations and the subgrid model

By using the three-dimensional LES turbulence model, the large-scale eddies are solved directly by the filtered Navier–Stokes equations, and the small eddies are modelled using a subgrid scale (SGS) model. The large-scale turbulence motions are strongly dependent on the flow geometry and boundary conditions, and they can be predicted by the resolved flow in the LES method. On the other hand, the subgrid scale model represents the small-scale eddy motion and is more universal in character than the large scale eddy. The filtering operation proceeds according to

$$\overline{\phi} = \frac{1}{\Delta}\int_{\Delta}\phi(x')dx', \quad x' \in \Delta, \tag{3.1}$$

$$G(x,x') = \begin{cases} 1/\Delta, & x' \in \Delta \\ 0, & \text{otherwise} \end{cases} \tag{3.2}$$

where Δ is the volume of a computational cell, and $G(x,x')$ is a filter function. As mentioned by Drikakis (2003) and Pope (2004), the filtered equations of this kind of conventional LES approaches are derived assuming the commutation between differentiated and filtered variables, and this assumption is valid only with equal filter length, which is not the case of complex geometry. It lacks the universality in the subgrid scale turbulence model. Recently, Drikakis et al. (2009), Hahn and Drikakis (2009a, b) developed implicit LES methodologies based on high-resolution methods with unfiltered equations to overcome the above difficulties. Nevertheless, referring to many reasonable successful previous studies using the conventional LES approaches (Chen et al., 2003; Liang and Papadakis, 2007; Afgan et al., 2007), we are convinced that this kind of simpler conventional LES method is suitable for the present study, considering the relatively simple geometry of the present simulation.

Applying the filtering operation, the incompressible Navier–Stokes equations for the evolution of the large-scale motions are obtained. The governing equations employed for LES are

$$\frac{\partial \overline{u}_i}{\partial x_i} = 0, \tag{3.3}$$

$$\frac{\partial \overline{u}_i}{\partial t} + \frac{\partial \overline{u}_i \overline{u}_j}{\partial x_j} = -\frac{1}{\rho}\frac{\partial \overline{p}}{\partial x_i} + \nu\frac{\partial^2 \overline{u}_i}{\partial x_j}\partial x_j - \frac{\partial \tau_{ij}}{\partial x_j} \quad (i=1,2,3) \tag{3.4}$$

where $\overline{u}_i$ are the filtered velocity components along the Cartesian coordinates x_i, $\overline{p}$ is the pressure, ρ is the fluid density and ν is the kinematic viscosity of the fluid. The influence of the small scales on the large (resolved) scales takes place through the subgrid scale stress defined by

$$\tau_{ij} = \overline{u_i u_j} - \overline{u}_i \overline{u}_j, \tag{3.5}$$

resulting from the filtering operation, which are unknown and must be modelled with a subgrid model. The majority of subgrid scale models are based on the eddy viscosity models of the following form:

$$\tau_{ij} - \frac{1}{3}\tau_{kk}\delta_{ij} = -2\nu_t \overline{S}_{ij}, \tag{3.6}$$

where the trace of the subgrid scale stresses τ_{kk} is incorporated in the pressure resulting in a modified pressure term, ν_t is the subgrid-scale kinematic viscosity, and $\overline{S}_{ij}$ is the strain rate tensor for the resolved scale defined by

$$\overline{S}_{ij} = \frac{1}{2}\left(\frac{\partial \overline{u}_i}{\partial x_j} + \frac{\partial \overline{u}_j}{\partial x_i}\right). \tag{3.7}$$

The most basic of subgrid scale models is proposed by Smagorinsky (1963) and has been further developed by Lilly (1966). In the Smagorinsky–Lilly model, the subgrid kinematic viscosity ν_t is modelled by

$$\nu_t = l_s^2 \left|\overline{S}_{ij}\right|, \tag{3.8}$$

where l_s is the mixing length for the subgrid scales, and $\left|\overline{S}_{ij}\right| \equiv \sqrt{2\overline{S}_{ij}\overline{S}_{ij}}$; l_s can be computed using

$$l_s = \min(ky, C_s\Delta^{1/3}), \tag{3.9}$$

where k is the von Kármán constant ($k = 0.42$) and y is the distance to the nearest wall. C_s is the Smagorinsky constant, and Δ is the volume of the computational cell.

It is known that the conventional LES is sensitive to the Smagorinsky constant. Lilly (1966) derived a value of 0.23 for C_s from homogeneous isotropic turbulence in the inertial subrange. However, this kind of large C_s value was found to cause excessive damping of the large-scale fluctuations in the presence of mean shear or in transitional flows, and small C_s values ($C_s < 0.1$) may cause convergence problems. For many investigators, the Smagorinsky constant ($C_s = 0.1$–0.14) has been found to yield good results for a wide range of flows. For example, the Smagorinsky constant, $C_s = 0.1$, was adopted by Chen et al. (2003) to investigate turbulent wake flows behind two side-by-side cylinders. Liang and Papadakis (2007) used $C_s = 0.1$ to investigate pulsating flow over a circular cylinder at subcritical Reynolds number. As a result, all computations in the present work were carried out with a Smagorinsky constant, $C_s = 0.1$, which is found to be a suitable value for the applications of the Smagorinsky model to turbulent wake simulation.

In the present simulation, the finite volume method applied on unstructured hexahedral grids is employed to calculate the three-dimensional unsteady incompressible Navier–Stokes equation. A second-order central differencing scheme is used for momentum discretization, while a second-order implicit scheme is employed to advance the equations to the new time level. The well-known pressure implicit method with splitting of operators (PISO) algorithm is used to deal with the pressure–velocity coupling between the momentum and the continuity equations.

3.2. Computational domain and boundary conditions

As shown in Fig. 1(a), U_∞ is the incoming mean flow velocity (in the x'-direction) and U_n (in the x-direction) is the velocity component normal to the axis of the cylinder. The yaw angle α is the angle between the incoming flow U_∞ and the direction normal to the cylinder axis. At the inlet boundary, uniform incoming flows with components $U_\infty \sin\alpha$ and $U_\infty \cos\alpha$ are imposed. As a result, the free-stream velocity has a component $U_n = U_\infty \cos\alpha$ normal to the cylinder and a component $U_\infty \sin\alpha$ tangential to the cylinder axis. A cylinder-based coordinate system is used in which the z-direction is oriented along the cylinder axis, the x-direction is parallel to the normal component U_n of the free-stream velocity, and the y-direction is normal to both the cylinder axis and the free-stream velocity. The computational boundaries are set at $24D_m$ and $16D_m$ in the x- and y-direction, respectively. The upstream boundary is set at $8D_m$ away from the centerline of the wavy cylinder. The downstream boundary is $16D_m$ away from the wavy cylinder. The spanwise domain of the wavy cylinder is set equal to two wavelengths '2λ' of the wavy cylinder (Fig. 1(b)). The Neumann-type boundary condition is used at the outlet boundary. A periodic boundary condition is employed at the boundaries in the spanwise direction (z-direction) of the cylinder. This is equivalent to treating the cylinder as an infinitely long cylinder. As a result, the end-wall effect is avoided. The no-slip boundary condition is prescribed at the surface of the cylinder. The lateral surfaces are treated as slip surfaces using symmetry boundary conditions. Similar boundary conditions were employed successfully by Lucor and Karniadakis (2003) for flow past a yawed cylinder.

In the present simulations, the Reynolds number based on the mean diameter D_m of wavy cylinder and the incoming flow U_∞ (in the x'-direction) is kept at $\mathrm{Re} = U_\infty D_m/\nu = 3900$ for all the cases studied. To simulate the 3-D wake flow accurately, the computational domain height in the cylinder spanwise direction should be larger than $3D_m$ (Kravchenko and Moin, 2000; Zhao et al., 2009). As mentioned by Lam and Lin (2007, 2008 and 2009), for a single wavy cylinder, periodic repetitive vortex structures were observed to be consistent with the periodic repetition of the cylinder's wavy surface at low Reynolds number ranging from 60 to 150, and also at a subcritical Reynolds number of 3000. In the present simulations, a wavy cylinder with a wavelength of $\lambda = 6D_m$ is adopted. The computational domain in the z-direction is set at $12D_m$ (2λ repeated with the periodic boundary condition imposed on the upper and lower ends). Considering the yaw angle and the incoming flow U_∞, the cylinder height (in the z'-direction) is from $12D_m$ to $6D_m$ corresponding to yaw angle α from 0 to 60°. Lucor and Karniadakis (2003) numerically investigated the oblique flow past a circular cylinder with α from 0 to 70° at $\mathrm{Re} = 1000$, the corresponding cylinder height in the x'-direction is from $22D_m$ to $7.5D_m$. Zhao et al. (2009) simulated flow around a yawed cylinder with a fixed cylinder height of $9.6D_m$ from $\alpha = 0°$ to 60° at $\mathrm{Re} = 1000$. It is anticipated that the present computational domain height ($12D_m$, in the z-direction) corresponding to the cylinder height with large yaw angle ($6D_m$, in the z'-direction) should be a suitable choice for the present simulations.

3.3. Grid impendence test

Grid independence test and the validation of numerical models are extremely important prior to extensive numerical simulations. Initially, the grid independence tests were carried out considering that the accuracy of the computational

results using LES is highly dependent on the mesh size and cell numbers. Fig. 1(c) shows that the computational domain is divided into a number of unstructured hexahedral grids. The grids are nonuniform in the x–y plane, but uniform along the z-direction. With regard to grid resolution requirements near the wall, the grids are clustered near the cylinder surface to resolve the viscous sub-layer of the near-wall region which corresponds to the distance from the cylinder surface to the nearest grid points is fixed at $y^+ \leq 1$and the spacing is properly increased at a ratio of 1.1 away from the cylinder surface. In the present simulation, three types of cylinder models with different cell numbers are calculated for both the circular and wavy cylinders. As shown in Table 1, for a circular cylinder with $\alpha = 0^\circ$, the results of mean drag coefficient $\overline{C}_D$ from the present LES calculations (CY-cases 2 and 3) are in good agreement with the LES values by Kravchenko and Moin (2000) and are close to the experimental or numerical results by Breuer (1998), Lubcke et al. (2001) and Franke and Frank (2002) at the same Reynolds number. They are also similar to results obtained by Norberg (1987) at Re = 3000 and the present experimental measurement performed at Re = 4000. The r.m.s. fluctuating lift coefficient C'_L values are all within the range of values summarized by Norberg (2001) and slightly smaller than the present experimental results due to the slight blockage effect on the experimental set-up. The Strouhal numbers St obtained by the present LES method are all in good agreement with both the LES and experimental results obtained by different investigators. For a wavy cylinder with $\alpha = 0^\circ$ (Table 2), the values of $\overline{C}_D$, C'_L and St of the WY-cases 2 and 3 are consistent with each other except for the results of the WY-case 1. To check the degree of accuracy of the numerical results, the power spectra of the lift coefficients for both unyawed circular cylinders and wavy cylinders with different grid sizes are plotted in Fig. 2. In general, consistent patterns can be observed in all flow regions for these three cases with different gird sizes. Moreover, the slope of the lift coefficient spectrum curve is shown to be in good agreement with a slope line of $-5/3$, similar to the lift coefficient power spectral obtained by Afgan et al. (2007). It also illustrated that the present solution is a grid converged solution. As a result, the cylinder cases 2 and 3 are all acceptable for the present simulation. To save computing time, the cylinder case 2 for both the circular and wavy cylinder cases are adopted for the present simulations.

For the study of force characteristics of yawed cylinders, the drag coefficient is normally defined as $C_D = 2F_D/\rho U_n^2 D_m H$ in the x-direction (direction parallel to the velocity component U_n) and the transverse lift coefficient is defined as $C_L = 2F_L/\rho U_n^2 D_m H$ [refer to Zhao et al. (2009)]; H is the computational domain height in the z-direction. The drag and lift are given by F_D in the x-direction andF_L in the y-direction, respectively. The Strouhal number based on the mean diameter D_m and the incoming flow U_∞ is defined as $\mathrm{St}_{(\alpha)} = fD_m/U_\infty$. Here, the

Table 1
Grid independence test for a circular cylinder at a yaw angle of $\alpha = 0^\circ$.

Case	Re	$\overline{C}_D$	C'_L	St
Norberg (1987) (Experimental)	3000	0.98–1.03	N/A	0.210–0.213
Breuer (1998) (LES) C1	3900	1.144	N/A	0.210–0.220
Kravchenko and Moin (2000) (LES)	3900	1.04	N/A	0.210
Lubcke et al. (2001) (Experimental)	3900	0.99	N/A	0.215
Franke and Frank (2002) (LES)	3900	0.994	N/A	0.209
Norberg (2001) (summarized)	3900	N/A	0.07, 0.3	0.208
Present (Experimental)	4000	1.03	0.16	N/A

Present LES cases	Cells	Re	$\overline{C}_D$	C'_L	St
CY-case 1	1 497 600	3900	1.073	0.164	0.207
CY-case 2	1 866 240	3900	1.041	0.114	0.208
CY-case 3	2 536 320	3900	1.033	0.121	0.211

Table 2
Grid independence test for a wavy cylinder at a yaw angle of $\alpha = 0^\circ$.

Case	Cells	$\overline{C}_D$	C'_L	St
WY-case 1	1 497 600	0.922	0.021	0.179
WY-case 2	1 866 240	0.897	0.013	0.184
WY-case 3	2 536 320	0.894	0.015	0.185

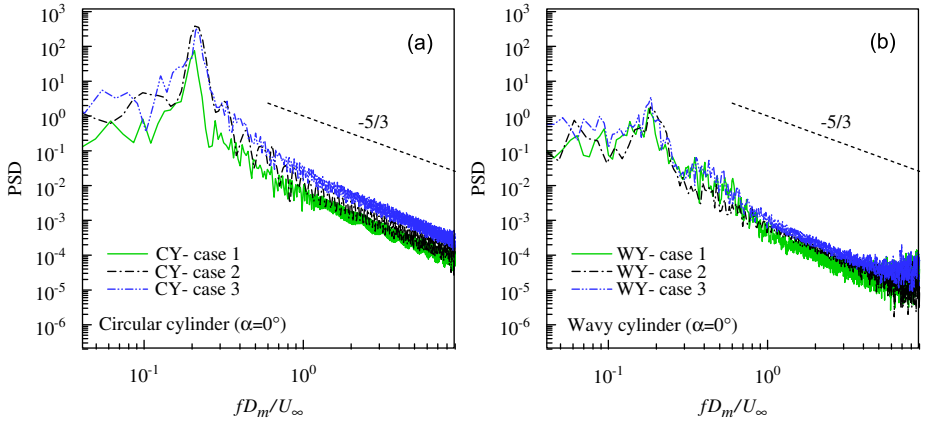

Fig. 2. Comparison of the lift coefficients power spectra of circular or wavy cylinders for different grid size cases shown on a log–log scale.

subscript (α) denotes the yaw angle of the cylinder. f is the frequency of vortex shedding which obtained by fast Fourier transform (FFT) of the time history of the fluctuating lift. A dimensionless time step $\Delta t U_\infty/D_m = 0.02$ was chosen for the present simulations, yielding a maximum CFL number close to 2 and ensuring a sufficiently small CFL number of less than 1 for most parts of the computational domain. The accuracy of the results was dictated by the numerical stability of the computations. So, a smaller time step in 0.005 was also tested. The differences in results between these two time step cases were found to be less than 2%. In the present simulations, at least 1500 dimensionless time steps, which corresponded to about 30 vortex-shedding cycles, were taken so as to obtain statistically more reliable information.

4. Experimental measurements

Experimental investigations have also been performed to validate the present numerical results. The Laser Doppler Anemometry (LDA) and load cell systems have been employed in a water tunnel and a wind tunnel, respectively.

4.1. LDA measurements

In order to obtain the quantitative mean and fluctuating velocity data around the yawed cylinder, a two-colour fiber-optic LDA system (DANTEC model 58N40 two-component LDA with enhanced FVA signal processor) were used in a closed-circuit water tunnel with a working section of 0.6 m × 0.3 m and a length of 2.4 m, corresponding to the direction of z', y' (transverse direction, the same as y-direction) and x' (streamwise direction of the test cylinder), respectively. The free-stream velocity in the testing area could be continuously adjusted from 0 to 4 m/s. The wavy cylinder of mean diameter $D_m = 0.02$ m (blockage ratio of 6.7%) was cantilever-mounted in the water tunnel. In the test section of the water tunnel, the distance between the cylinder lower end and the bottom wall of the water tunnel is about 0.005 m, resulting in an aspect ratio of the cylinder of 29 in the z'-direction [refer to Fig. 1(a)]. The experimental uncertainties are estimated to be less than 3% for the mean velocity and a corresponding error of less than 7% for the root mean square values. The LDA measurements were carried out at difference streamwise positions (in the x'-direction) of the flow field. For each data-point, 50 000 validated samples were acquired with a data rate of 0.8–4 kHz. The oncoming mean flow velocity U_∞ is set at 0.2 m/s, corresponding to the Reynolds number of 4000 with the free-stream turbulent intensity of less than 2%.

4.2. Load cell measurements

For force measurement, the experimental cylinder models were placed in a recirculation wind tunnel system with a working square cross-section (0.6 m × 0.6 m) and a length of 2.0 m. A 3-axis piezoelectric load cell (Kistler Model 9251) was used to measure the force on the cylinders. The mean stream velocity in the wind tunnel system could be continuously adjusted from 0 to 40 m/s by an inverter, which controls the rotation speed of the wind tunnel fan. The

load cell mounted on the top end of the cylinder is bolted tightly between two stainless machine-polished steel blocks. It is able to measure the instantaneous integral fluid forces acting over the span of the cylinder exposed inside the wind tunnel. To avoid the wind tunnel vibration effect on the measurements, the load cell holder was mounted on an external rigid support detached from the wind tunnel. Static calibrations of the load cell in the lift and drag directions were carried out using dead weights. The load and output voltage relation of the load cell was linear.

Assuming a uniform wind load distribution along the cylinder, the load cell can measure simultaneously the two force components on the cylinder, including the time averaged drag and lift, and their root mean square values. Force measurements were performed at three Reynolds numbers of 4000, 10 600 and 20 100, respectively. At this Re range, the maximum longitudinal turbulent intensity was 0.7% in the free-stream, and the velocity was uniform to within 2%. The wavy cylinder of mean diameter $D_m = 0.02$ m, causing the maximum blockage is about 4%, and a test aspect ratio of 30. The distance between the cylinder lower end and the bottom wall is about 0.003 m with no end plate mounted on the cylinder. The end-effect test showed that there were negligible changes in forces on the cylinder due to the lower end of the cylinder being within the low-speed wall boundary layer, whose thickness was estimated to be about 0.015 m at $U_\infty = 8$ m/s, (also, refer to Alam and Zhou, 2007). Considering the present experimental conditions and the model set-up, the load cell uncertainties is estimated to be $\pm 5\%$ for drag measurement, while is about $\pm 10\%$ for the measurement of fluctuating lift in such flow conditions.

5. Results and discussion

5.1. Flow patterns and velocity distributions

Fig. 3 shows a comparison of flow past a yawed circular cylinder at $\alpha = 45^\circ$ between the present LES result at Re = 3900 and the DNS result at Re = 1000 by Zhao et al. (2009). The 3-D streamlines behind the wake of circular cylinder show two directions of motion. One kind of streamlines move in the streamwise direction (x'-direction, parallel to the direction of U_∞), while others show a bend behind the cylinder and then move in the spanwise direction of the cylinder (z'-direction). This kind of motion characteristic is due to the spanwise velocity component producing a bending streamline pattern. The present LES results show good agreement with the flow visualization by Kozakiewicz et al. (1995) and the DNS result by Zhao et al. (2009) at similar Reynolds number range.

Fig. 4(a–c) further illustrates the accuracy of the present LES results for flow past circular cylinders with yaw angles of $\alpha = 0^\circ$, 30° and 60°, respectively. The 3-D spanwise vortex structures (ω_z) of the yawed circular cylinders captured by the present LES method show similar characteristics with those flow visualization results by Thakur et al. (2004). The wavy cylinders with yaw angles of 0, 30 and 60° have been included for comparison and discussion (Fig. 4(d–f)). For unyawed circular and wavy cylinders (Fig. 4(a, d)), the 3-D instantaneous wake structures show periodic vortex shedding characteristics behind the cylinders. The spanwise vortex structures are parallel to the axis of both the circular cylinder and the wavy cylinder. For the wavy cylinder with $\alpha = 0^\circ$ (Fig. 4(d)), the periodic repetitive near-wake structures along the spanwise direction (z-direction) still occur and are similar to those found at low Reynolds numbers (Lam and Lin, 2007, 2009). It can be clearly observed that the roll-up of the free shear layer behind such wavy cylinder also occurs further downstream compared to a circular cylinder. This is partly due to the spanwise flow motion from saddle position to nodal position of the wavy cylinder (Lam and Lin, 2008). As the yaw angle increases to $\alpha = 30^\circ$, for a circular cylinder, the 3-D spanwsie vortex structures are still basically parallel to the axis of the cylinder (Fig. 4(b)). For a wavy cylinder, however, the flow generates a far more complicated structure at such a yaw angle compared with that

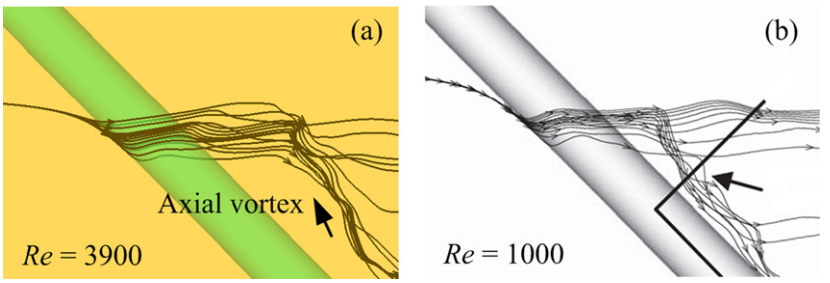

Fig. 3. Comparison of the wake flow of a circular cylinder with $\alpha = 45^\circ$: (a) present LES results of streamlines and (b) DNS results of streamlines by Zhao et al. (2009).

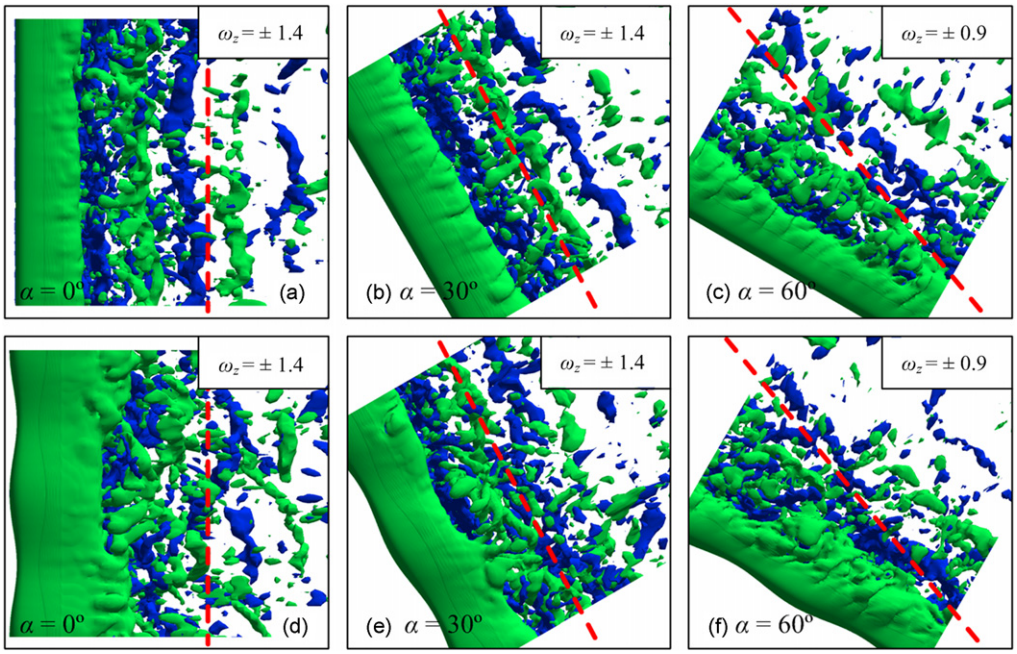

Fig. 4. Instantaneous spanwise vortex structures for $\alpha = 0°$, 30 and 60°, respectively: (a–c) for circular cylinders and (d–f) for wavy cylinders.

of a circular cylinder (Fig. 4(e)). Along the spanwise direction, the wake structures show certain evident waviness for the yawed wavy cylinder. This means that the near-wake free shear layers are very unstable. With further increase of the yaw angle to $\alpha = 60°$, it is interesting to note that the spanwise wake structures of a circular cylinder are no longer parallel to the axis of the cylinder but they are inclined at an angle smaller than the yaw angle of the cylinder (Fig. 4(c)). Similar flow visualization results had been observed by Ramberg (1983) at $\alpha > 45°$ and Lucor and Karniadakis (2003) at $\alpha = 70°$, and the flow visualization results by Thakur et al. (2004). The well-organized wake structures, in general, were broken down for the wavy cylinder at $\alpha = 60°$. With a large yaw angle, the free shear layers roll-up close to the back of the wavy cylinder like those of a circular cylinder at the same flow condition (refer to Fig. 4(f)). Consequently, the advantageous effects on the control of vibration and drag of a wavy cylinder also reduce at large yaw angle.

The normalized mean velocity (U'/U_∞) and the normalized r.m.s. values of the fluctuating velocity ($u'_{\mathrm{rms}}/U_\infty$) distributions along the wake centerline ($y = 0$, x'-direction) are plotted in Figs. 5 and 6 for both circular cylinders and wavy cylinders with yaw angles at $\alpha = 0°$, 15°, 30° and 45°, respectively. The velocity distributions of the present LES at $\mathrm{Re} = 3900$ are close to the experimental measurements which were obtained by the present LDA technique at $\mathrm{Re} = 4000$. Typically, for an unyawed circular cylinder as shown in Fig. 5(a), the time-averaged centreline velocity of a circular cylinder at $\mathrm{Re} = 3900$ from the experiments of Lourenco and Shih, Ong and Wallace (data both taken from Kravchenko and Moin (2000)) have been included for the validation on the accuracy of the present LDA measurement. The experimental data at $\mathrm{Re} = 3900$ by Govardhan and Williamson (data taken from Ma (2000)) were also added. In the figure, it can be seen that the present LDA results show good agreement with those by Lourenco and Shih, Ong and Wallace for $x'/D_m > 3$. However, all the experimental results are different in the near-wake of the cylinder, especially so for the results by Govardhan and Williamson. As discussed by Ma (2000), the aspect ratio in the Lourenco and Shih experiment was 20.5 while in the Govardhan and Williamson experiments it was 10, and it is 29 in the present experiment, which may be the reason for the difference in the formation length obtained.

As shown in Fig. 5(a), three distinctive different velocity distribution curves of U'/U_∞ for unyawed circular cylinder, wavy cylinder (nodal plane) and wavy cylinder (saddle plane) are plotted. Along the spanwise direction of the wavy cylinder, the lengths of the vortex formation regions (negative velocity region) at the saddle planes are shorter than that at the nodal plane U'/U_∞. In general, the vortex formation length for the wavy cylinder is clearly longer than that of the circular cylinder. Lam and Lin (2008) pointed out that the mean drag coefficient $\overline{C}_D$ at subcritical Reynolds numbers for both unyawed wavy and circular cylinders are inversely proportional to the average vortex formation lengths [the location of the time-averaged closure point ($U'/U_\infty = 0$) of streamwise velocity (x'-direction) on the wake

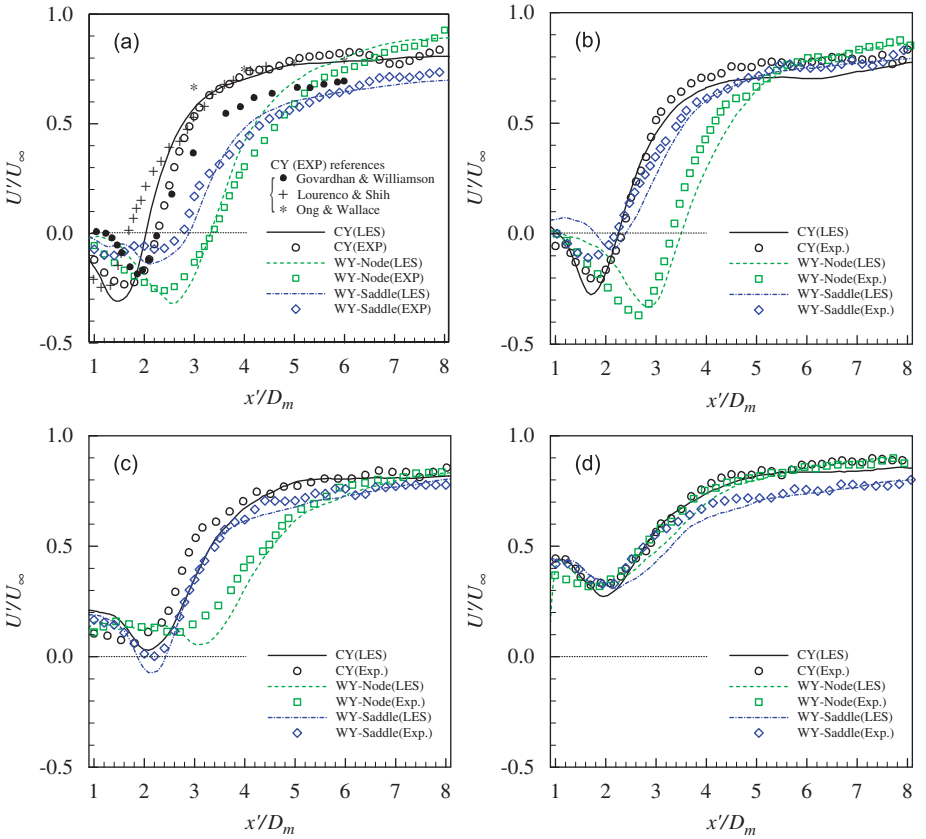

Fig. 5. Time-averaged mean streamwise velocity distributions along the wake centreline ($y = 0$, x'-direction) at (a) $\alpha = 0^\circ$, (b) $\alpha = 15^\circ$, (c) $\alpha = 30^\circ$ and (d) $\alpha = 45^\circ$.

centerline, $y = 0$]. That is to say, the evidently longer vortex formation region is the main cause for the reduction of mean drag and the suppression of fluctuating lift.

Increasing the yaw angle to $\alpha = 15^\circ$, only slight differences in the velocity distributions between circular cylinder cases with yaw angles of $\alpha = 0^\circ$ and 15° are obtained (Fig. 5(b)). The width of the recirculation zone (negative velocity region) becomes wider than that of the circular cylinder case at $\alpha = 0^\circ$. The distributions of U'/U_∞ in the near-wake of the wavy cylinder's nodal position at $\alpha = 15^\circ$ are similar to the wavy cylinder case with $\alpha = 0^\circ$; while at the saddle position, the U'/U_∞ for wavy cylinder is close to that of a circular cylinder at $\alpha = 15^\circ$. As shown in Fig. 5(c), it is interesting to note that the flow-reversing region behind both the wavy and circular cylinders has greatly diminished and sometimes it disappears completely. At $\alpha = 30^\circ$, the flow component of $U_\infty \sin\alpha$ increases significantly. As a result, the velocity distribution is much different from that of the smaller yaw angle cylinders. The curves for the distributions of U'/U_∞ in the wake of nodal and saddle positions of the wavy cylinder become closer to each other. Fig. 5(d) shows that the velocity distributions along the wake centreline of the yawed wavy and circular cylinders at $\alpha = 45^\circ$ are nearly overlapping on each other on many parts of the curves. No significant variation is captured from the nodal plane to the saddle plane of the yawed wavy cylinder. The similarity of velocity distributions along the wake centreline for the yawed wavy and circular cylinders implies that there are but small differences in the effect of drag reduction and the suppression in the fluctuating lift at such a large yaw angle. It can be concluded that one of the effects of yaw angle is that it shortens the length of the recirculation zone (vortex formation length) of the wavy cylinder.

Similar trends have been found in the characteristics of the fluctuating velocity distributions (corresponding to the turbulence intensity) for yawed wavy and circular cylinders. Fig. 6 shows the length of maximum turbulence intensity position (the position of maximum $u'_{\mathrm{rms}}/U_\infty$ along the wake centerline) and the maximum value of turbulence intensity along the wake centerline. For unyawed wavy cylinder, the values of turbulence intensity of both the nodal and saddle positions are all smaller than that of an unyawed circular cylinder (Fig. 6(a)). Lam and Lin (2008) concluded that a longer maximum turbulence intensity length and lower values of turbulence intensity would have an obvious advantage

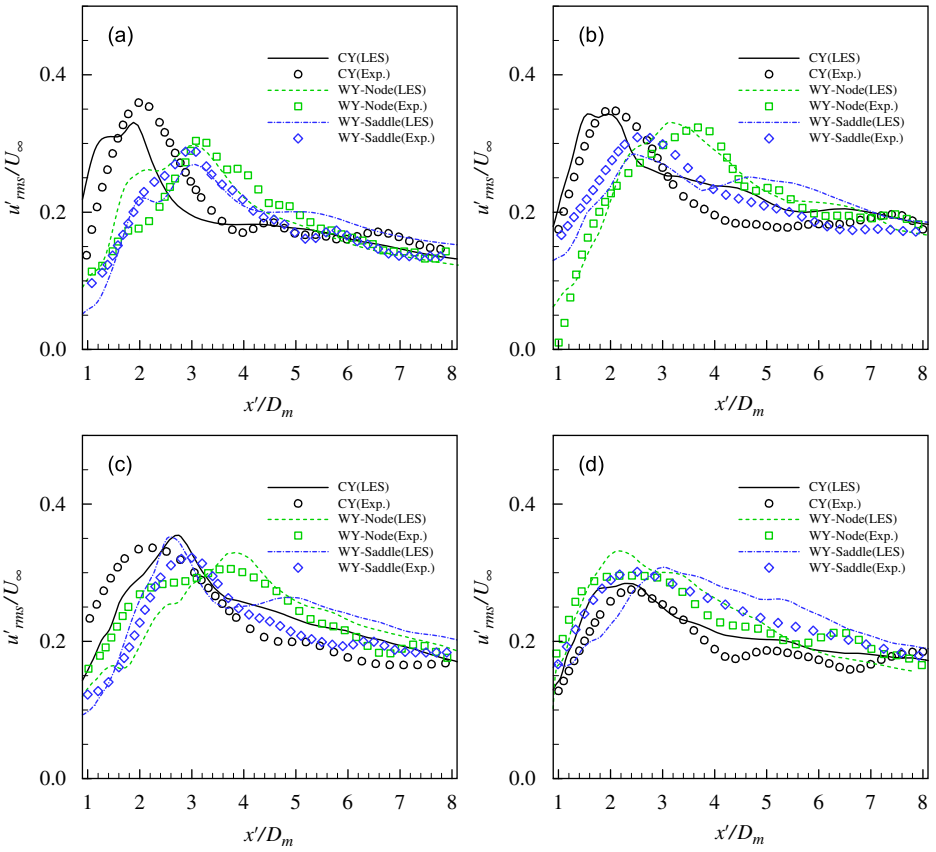

Fig. 6. Time-averaged fluctuating streamwise velocity (r.m.s. value) distributions along the wake centreline ($y = 0$, x'-direction) at (a) $\alpha = 0^\circ$, (b) $\alpha = 15^\circ$, (c) $\alpha = 30^\circ$ and (d) $\alpha = 45^\circ$.

on the minimization of fluctuating lift. That means the unyawed wavy cylinder with large wavelength has a beneficial effect on the control of the lift fluctuation. With a yaw angle of $\alpha = 15^\circ$, the turbulence intensity $u'_{\mathrm{rms}}/U_\infty$ of a circular cylinder is similar to that of the unyawed case; however, the peak value becomes smaller. The difference of turbulence intensity $u'_{\mathrm{rms}}/U_\infty$ at a yaw angle of $\alpha = 15^\circ$ between wavy and circular cylinders is reduced. These kinds of flow characteristics make the wake pattern behind the yawed wavy cylinder to exhibit a more complicated structure than that of a circular cylinder. Nevertheless, at such small yaw angle of $\alpha \leq 15^\circ$, the wavy cylinder still has a positive effect on drag reduction and vibration control (Fig. 6(b)). However, as shown in Fig. 6(c, d), the turbulence intensity $u'_{\mathrm{rms}}/U_\infty$ distributions for the yawed wavy cylinder are close to that of a circular cylinder at the same yawed angle ($\alpha = 30^\circ$, 45°). This is particularly true for the yawed cylinders at $\alpha = 45^\circ$. It means that the effects of a wavy cylinder for drag reduction and fluctuating lift suppression are insignificant at such yaw angles compared with a corresponding yawed circular cylinder.

Fig. 7 shows the instantaneous wake patterns of circular and wavy cylinders in the x–y plane with yaw angles from $\alpha = 0^\circ$ to 45°. For the circular cylinder, the length of the recirculation zone behind the cylinder does not exhibit a large variation with the increase of yaw angle up to $\alpha = 45^\circ$ (Fig. 7(a–d)). This means that the free shear layer for wake vortex shedding is still approximately parallel to the axis of the circular cylinder. Referring to Fig. 4(a, b), it can also be observed that the spanwise vortex structures are still approximately parallel to the cylinder and approach a so called quasi-two-dimensional flow pattern along the spanwise direction. For unyawed wavy cylinder, due to the wavy separation line (Lam and Lin, 2008, 2009), the free shear layer behind the nodal and saddle positions extends further downstream (Fig. 7(e, i)). The recirculation zone is much larger than that of a circular cylinder, resulting in an evident drag force reduction and vibration suppression. Unlike for a circular cylinder, when the yaw angle of wavy cylinder is increased to 15°, the wake pattern shows some gradual changes compared with the unyawed wavy cylinder (Fig. 7(f, j)). Increasing the yaw angle to 45°, the length of the recirculation zones behind the wavy cylinder in the nodal and saddle

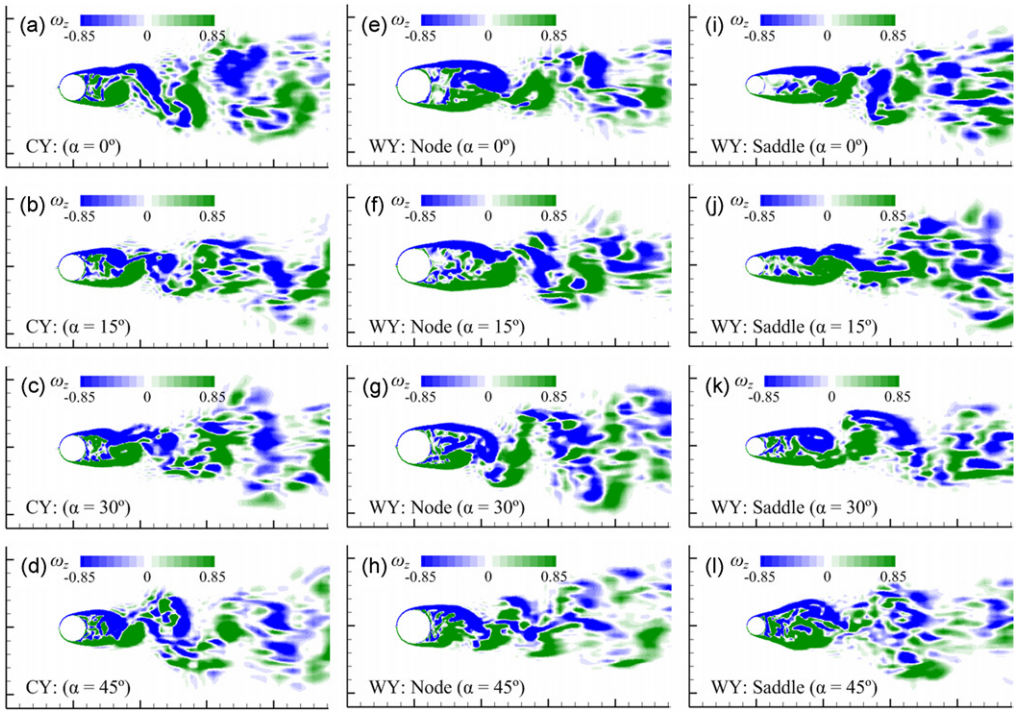

Fig. 7. Instantaneous wake patterns of circular or wavy cylinders in the x–y plane ($\alpha = 0$, 15, 30 and 45°): (a–d) for circular cylinders, (e–h) in nodal plane of wavy cylinders and (i–l) in saddle plane of wavy cylinders.

positions is reduced significantly (Fig. 7(h, l)). The wake patterns are much more different with the wavy cylinder at smaller yaw angle. The difference in the length of the recirculation zone between wavy and circular cylinders becomes quite obvious at the yaw angle of 45°. This means more complicated flow structures with stronger 3-D effect on the wavy cylinder are generated and the near-wake free shear layers become very unstable. It also implies that the advantageous effects of long vortex formation length of wavy cylinders have disappeared. Finally, the near-wake vortex structures are strongly distorted, with the disappearance of the clear vortex patterns. Moreover, the wakes behind saddle positions become wider than those behind the nodes of wavy cylinder with $\alpha = 45°$, which are opposite for that of unyawed wavy cylinder.

As shown in Fig. 8, with a large yaw angle of $\alpha = 60°$, the mean streamwise velocity for both the yawed wavy and circular cylinders show no reverse flow in the streamwise direction in the near-wake. This implies a strong spanwise velocity motion occurring near the wake of the cylinder, which also reduces the intensity of the fluctuating streamwise velocity. In general, the time-averaged velocity distributions show little difference between the wavy and circular cylinders at such large yaw angle. Typically for the yawed wavy cylinder, the difference of velocity distributions between the nodal and saddle planes disappears generally. As a result, the periodic vortex structures along the cylinder spanwise direction are destroyed.

Fig. 9 shows the instantaneous wake patterns of wavy and circular cylinders with a very large yaw angle of $\alpha = 60°$. The cross-section spanwise vortices show a nonuniform vortex pattern along the spanwise direction (z-direction) for the yawed circular cylinder. It can be clearly seen that, at a particular instant, at $z/D_m = 12$ plane (x–y plane), the recirculation zone behind the circular cylinder is much larger than that at other positions. The positions of the centre of vortices 1, 2 and 3 are also far away from the cylinder with the free shear layer extending to the further downstream position. Then the recirculation zone is gradually reduced with the decrease of the position of z/D_m (Fig. 9(a–d)). In contrast to that being shown in Fig. 4(c), in general, the 3-D wake structure of the yawed circular cylinder is no longer parallel to the cylinder axis, with a shedding angle smaller than the yaw angle and it is stable in space and time. This characteristic is similar to which reported by Lucor and Karniadakis (2003). Ramberg (1983) pointed out that for a yaw angle larger than 45°, the spanwise wake patterns oriented with a smaller angle than the yaw angle of the circular cylinder. It is consistent with what was observed in the present simulations (for a circular cylinder with a yaw angle up

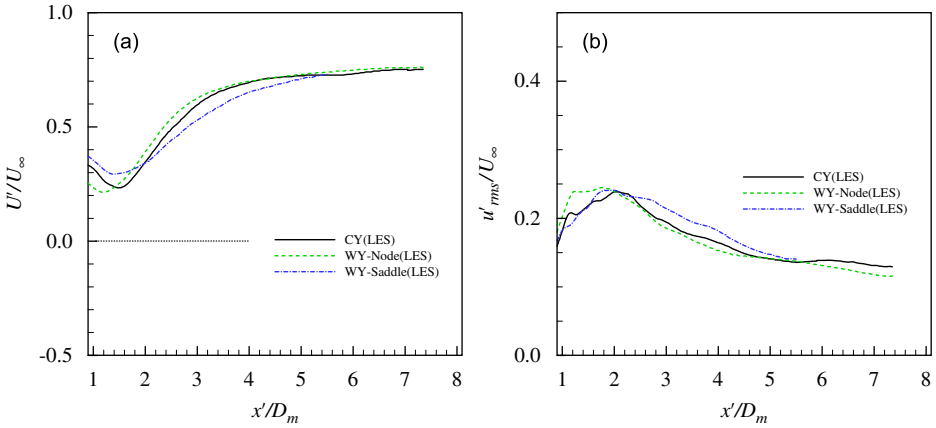

Fig. 8. Time-averaged velocity distributions along the wake centerline ($y = 0$, x'-direction) at $\alpha = 60°$: (a) mean streamwise velocity and (b) fluctuating streamwise velocity (r.m.s. value).

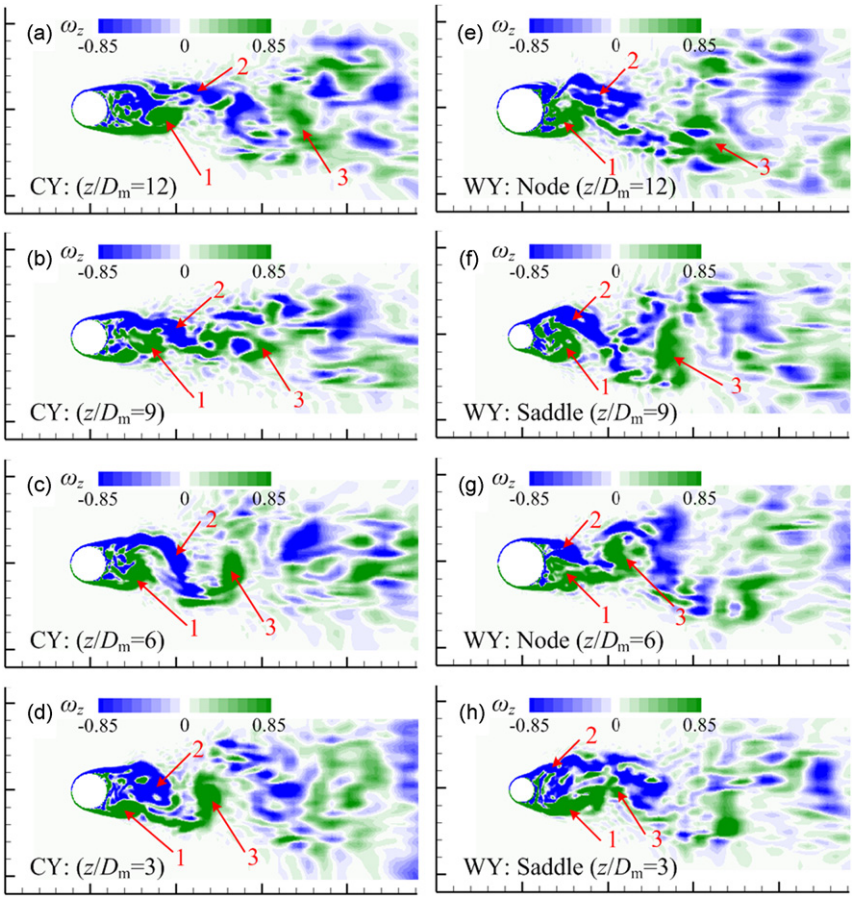

Fig. 9. Instantaneous wake patterns of circular or wavy cylinders in the x-y plane ($\alpha = 60°$): (a–d) circular cylinder and (e–h) wavy cylinder.

to 45°, the wake patterns are still parallel to the axis of the cylinder). This kind of regularity is broken when the yaw angle is further increased to 60°. As shown in Fig. 9(e–h), at a yaw angle of 60°, the recirculation zone in each cross-sectional plane of the wavy cylinder is of nearly equal length. The length is much shorter than that for 0° yaw angle for

both of the wavy and circular cylinders, and this will result in an increase of the drag force (refer to Fig. 7). Similar to the yawed circular cylinder, the flow pattern behind the 60° yawed wavy cylinder is not parallel to the cylinder axis, with much more complex wake structures (refer to Fig. 4(f)). Unlike the unyawed wavy cylinder, the flow separation characteristics along the spanwise direction have changed. Such a large yaw angle makes the vortex shedding very irregular. It also means that an increase of fluctuating pressure and force would occur.

5.2. Pressure and velocity distributions in x–z planes

The instantaneous and time-averaged mean velocity vector distributions (enlarged in zoom-in pictures) around the yawed circular and wavy cylinders overlaid on the contours of pressure distributions in x–z plane at $y = 0$ positions are plotted in Figs. 10–12. The instantaneous pressure coefficient is defined as $C_p = (P - P_\infty)/(\rho U_\infty^2/2)$ (P is the static pressure in x–z plane and P_∞ is the oncoming flow static pressure) and $\overline{C}_p$ is the time-averaged mean pressure coefficients. As shown in Fig. 10, for the unyawed wavy cylinder, the spanwise flow in the cylinder centreline section of $y = 0$ (x–z plane) shows significant orderly motion from nodal positions to saddle positions at both the front and the rear mean stagnation line, compared with the irregular spanwise flow motion behind the unyawed circular cylinder, as shown by the zoom-in pictures [also refer to Williamson (1996)]. This gives a good illustration of the well-organized and spanwise periodic repetitive wake structures generated behind the wavy cylinder. Furthermore, the values in the $\overline{C}_p$ distributions on the rear face of the wavy cylinder are much higher than for the corresponding circular cylinder. Lam and Lin (2008) stated that for a wavy cylinder at Re = 3000, the mean drag coefficient is generally proportional to the negative value of $\overline{C}_p$. This means that the higher value of $\overline{C}_p$ distribution on the rear face of a wavy cylinder may result in a smaller value of drag generation on the cylinder compared with a circular cylinder at the same flow conditions. At yaw angle $\alpha = 30°$, due to the additional oncoming flow component in spanwise direction ($U_\infty \sin\alpha$), the typical spanwise flow motion on the wavy cylinder from node to saddle has been modified as shown in the zoom-in picture. However, the well-organized spanwise periodic repeated 3-D vortex structures still exist, and the pressure difference

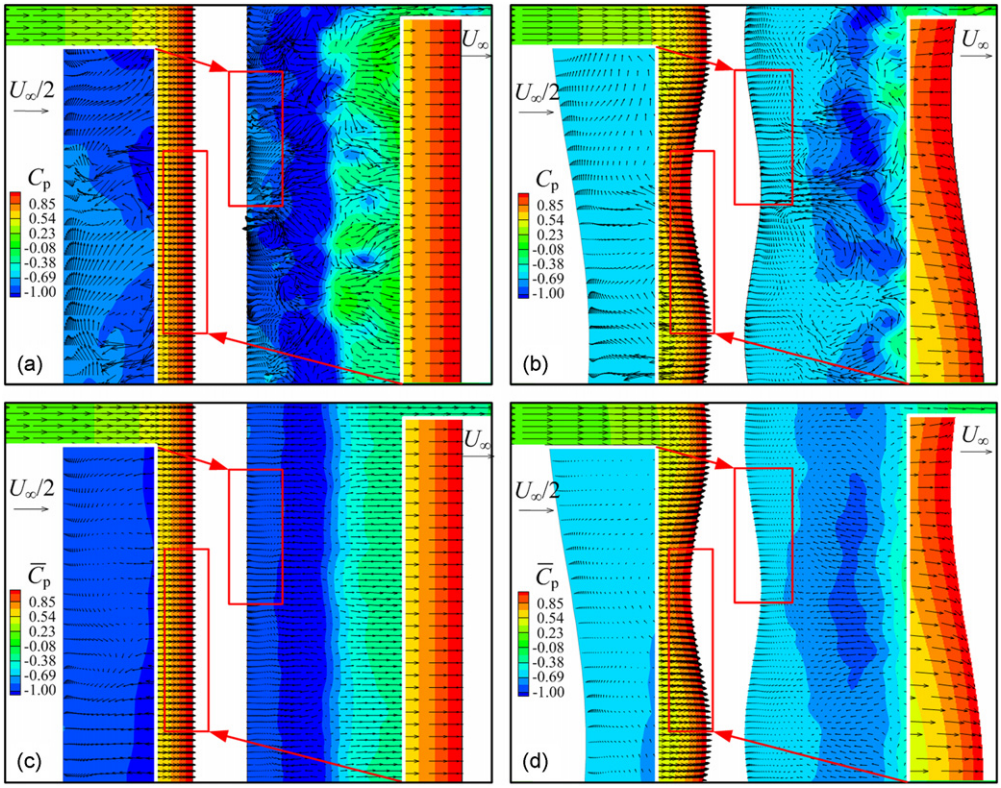

Fig. 10. Velocity vector distributions overlaid on contours of pressure coefficient in x–z plane at $y = 0$ with $\alpha = 0°$: (a) circular cylinder with instantaneous values, (b) wavy cylinders with instantaneous values, (c) circular cylinder with time-averaged values and (d) wavy cylinders with time-averaged values.

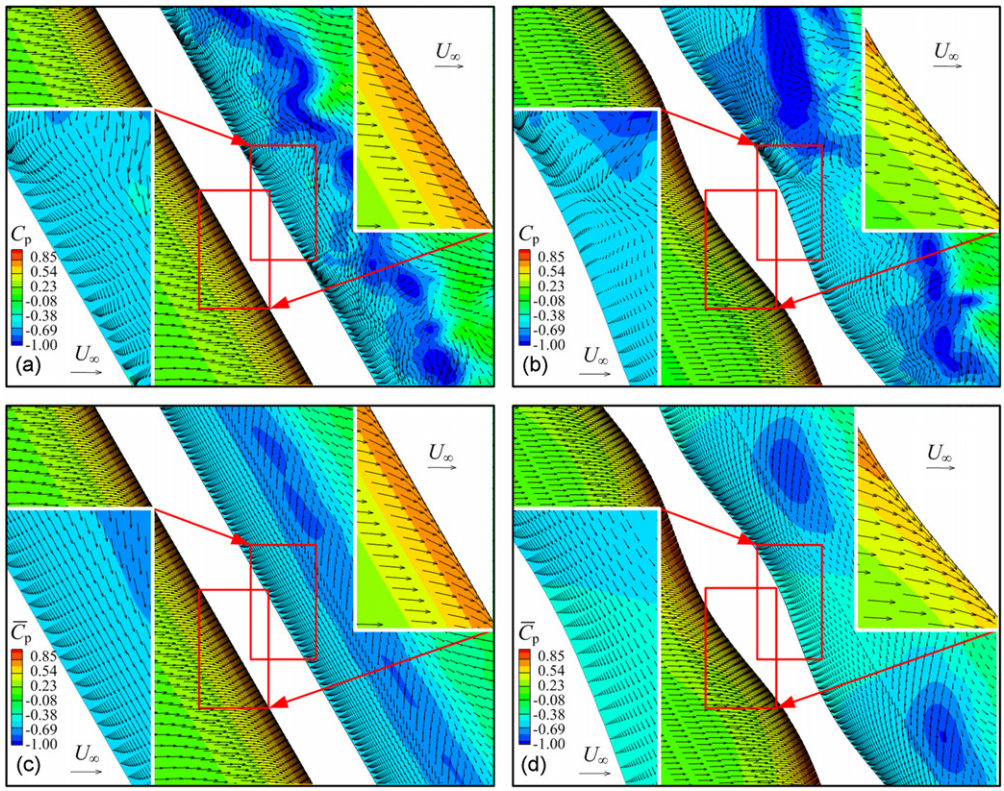

Fig. 11. Velocity vector distributions overlaid on contours of pressure coefficient in x–z plane at $y = 0$ with $\alpha = 30°$: (a) circular cylinder with instantaneous values, (b) wavy cylinders with instantaneous values, (c) circular cylinder with time-averaged values and (d) wavy cylinders with time-averaged values.

between the frontal surface and rear surface of the yawed wavy cylinder is smaller than that of the circular cylinder (Fig. 11). Further increasing the yaw angle to $\alpha = 60°$, the significantly increased spanwise oncoming flow component ($U_\infty \sin \alpha$) has suppressed the typical spanwise flow motion (node to saddle) behind the wavy cylinder (Fig. 12). As a result, the wake structures behind the wavy cylinder have been greatly altered with the disappearance of the characteristics of the periodic 3-D wake structures. Furthermore, the pressure distributions show little difference between the wavy and circular cylinder at such larger yaw angles. That is to say, such a yawed wavy cylinder no longer produces the desired effect on drag reduction control as compared with the circular cylinder.

5.3. Force characteristics and Strouhal numbers

Lam and Lin (2009) simulated flow past a wavy cylinder with $\lambda/D_m = 6$ and $a/D_m = 0.15$ at Re = 100 and obtained a drag reduction of around 18% with full suppression of the fluctuating lift force. At subcritical Reynolds numbers, similar to the results obtained by Lam et al. (2010), also refer to the present Tables 1 and 2, the mean drag coefficient $\overline{C}_D$ and fluctuating lift coefficient C'_L of such a wavy cylinder show significantly smaller values than those of a circular cylinder within the same Reynolds number range. A drag reduction of up to 14% was obtained. Also more than 80% reduction of fluctuating lift coefficients was achieved. These results confirmed that the wavy cylinder with such wavelength ($\lambda/D_m = 6$, $a/D_m = 0.15$) is a suitable choice for suppression of cylinder vibration and drag reduction in the subcritical Reynolds number regimes as well.

Fig. 13 shows the mean drag coefficients and fluctuating lift coefficients for circular and wavy cylinders at different yaw angles. The experimental results measured by the load cell technique at Reynolds numbers of 4000, 10 600 and 20 100 have been added for comparison and discussion. The present experimental results for an unyawed circular cylinder agree well with those summarized by Zdravkovich (2003). The values of $\overline{C}_D$ by LES methods for all wavy and circular cylinder cases at Re = 3900 are close to the present experimental measurements at Re = 4000 (Fig. 13(a, b)); while the values of C'_L for the present LES are slightly lower than the experimental results (Fig. 13(c, d)). This may be

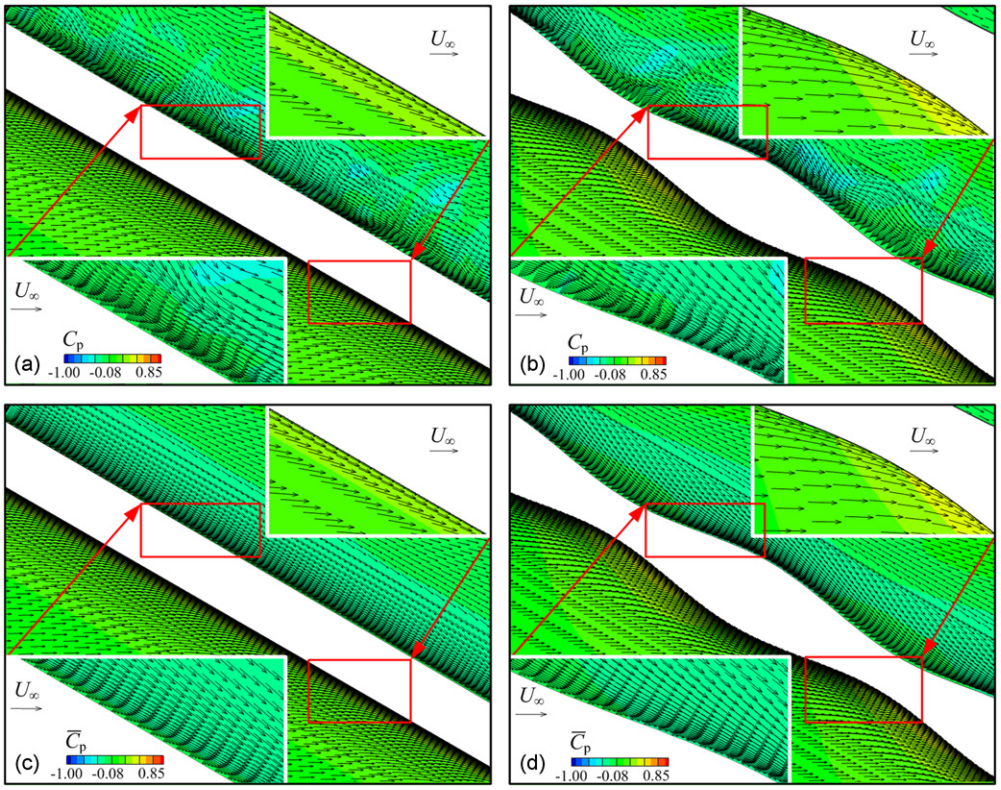

Fig. 12. Velocity vector distributions overlaid on contours of pressure coefficient in x–z plane at $y = 0$ with $\alpha = 60°$: (a) circular cylinder with instantaneous values, (b) wavy cylinders with instantaneous values, (c) circular cylinder with time-averaged values and (d) wavy cylinders with time-averaged values.

due to the no-slip end-wall effect for the finite length of the cylinder, compared with the computational domain adopted with periodic boundary condition on the up and down surfaces. Nevertheless, the present results on force characteristics for both the LES and load cell methods are all very close to each other. For the circular cylinder with yaw angle less than 45°, the values of $\overline{C}_D$ and C'_L show little variation with change of yaw angle; while the values of $\overline{C}_D$ and C'_L increase visibly when the yaw angle becomes greater than 45° (Fig. 13(a, c)). For the wavy cylinder (Fig. 13(b, d)), however, the values of $\overline{C}_D$ and C'_L increase with increasing yaw angle. In general, the values of $\overline{C}_D$ and C'_L of the yawed wavy cylinder are all less than those of corresponding circular cylinders at the same flow conditions with $\alpha \leq 45°$. But this trend is gradually reduced with increasing yaw angle. At $\alpha = 60°$, only a slight drag reduction can be seen for the wavy cylinder, with less vibration suppression compared with the yawed circular cylinder.

Fig. 14 shows the ratio of $\overline{C}_D/\overline{C}_{D(\alpha=0°)}$ for yawed wavy and circular cylinders. Here, the subscript ($\alpha = 0°$) denotes the cylinder with unyawed angle. As shown in Fig. 14(a), the values of $\overline{C}_D$ for yawed circular cylinders obtained by the LES method and load cell measurements are generally consistent with that predicted by the Independence Principle of the circular cylinder with a yaw angle $\alpha \leq 45°$. For yawed wavy cylinder, however, the value of $\overline{C}_D$ does not obey exactly the Independence Principle for circular cylinders (Fig. 14(b)). Due to the variation of surface cross-sections of the wavy cylinders and the evident spanwise flow motion, the flow separation lines have been changed. This may lead to an increase in instability of the near-wake vortex structures, and as a result the behaviour breaks away from the Independence Principle curve as soon as α becomes greater than 15°.

Fig. 15 shows the Strouhal numbers (based on the incoming flow in the x'-direction, U_∞) $\mathrm{St}_{(\alpha)} = fD_m/U_\infty$ with the power spectra of the lift coefficients of circular and wavy cylinders at three yaw angles. Here, the subscript (α) denotes the yaw angle of the cylinder. The Strouhal numbers of the wavy cylinders are in general smaller than those of circular cylinders. With increasing yaw angle, the value of the Strouhal number is reduced. If the definition of Strouhal numbers is based on the flow component normal to the axis of the cylinder (x-direction) with $\mathrm{St}_{n(\alpha)} = fD_m/U_n$ [refer to Zhao et al. (2009)], the value of Strouhal number for circular cylinders with yaw angles of 0, 30 and 60° will be changed to $\mathrm{St}_{n(\alpha)} = 0.208$, 0.211 and 0.260, respectively. They are close to the numerical simulation values of 0.22, 0.24 and 0.28

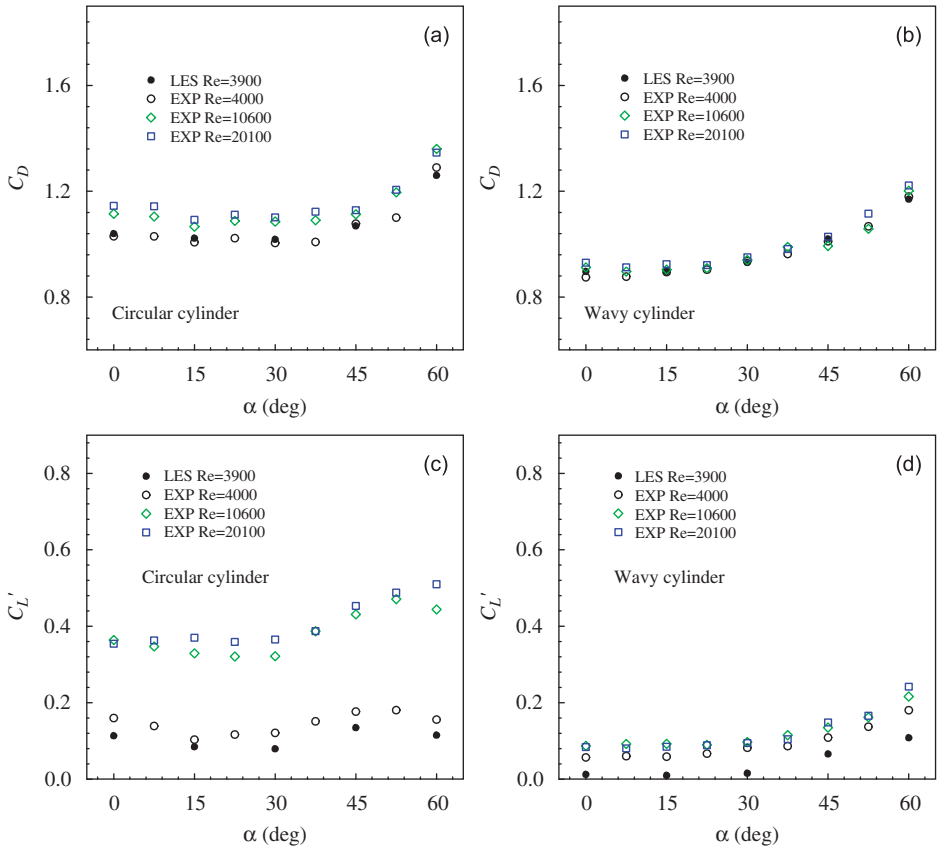

Fig. 13. Mean drag coefficients and fluctuating lift coefficients (r.m.s.) values for circular or wavy cylinders at different yaw angles.

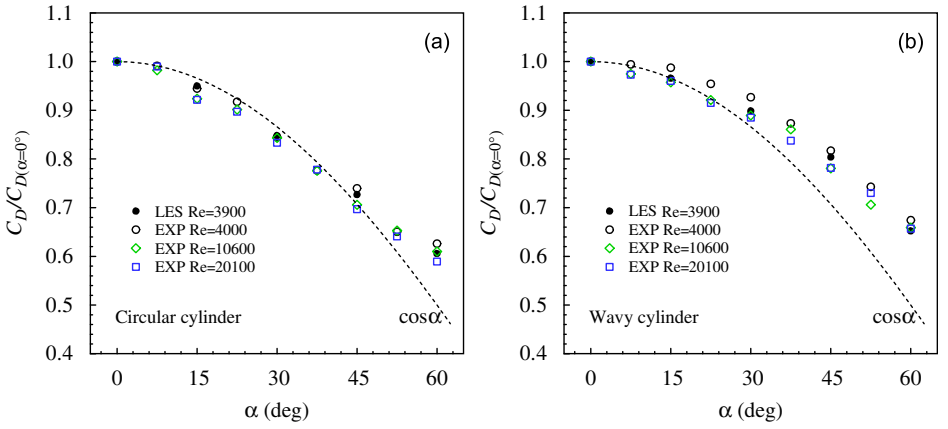

Fig. 14. The ratio of mean drag coefficients for yawed circular cylinders or wavy cylinders.

obtained by Thakur et al. (2004) and the experiments by Van Atta (1968), who cites Strouhal numbers of 0.20, 0.21 and 0.28 for the three yaw angles; while for wavy cylinders at $\alpha = 0°$, $30°$ and $60°$, the Strouhal number is $St_{n(\alpha)} = 0.184$, 0.218 and 0.232, respectively. This means that the vortex shedding will be enhanced by increasing the yaw angle, typically for the cylinder cases with large yaw angles. It also partly explains why the values of $\overline{C}_D$ and C_L' increased significantly with $\alpha = 60°$.

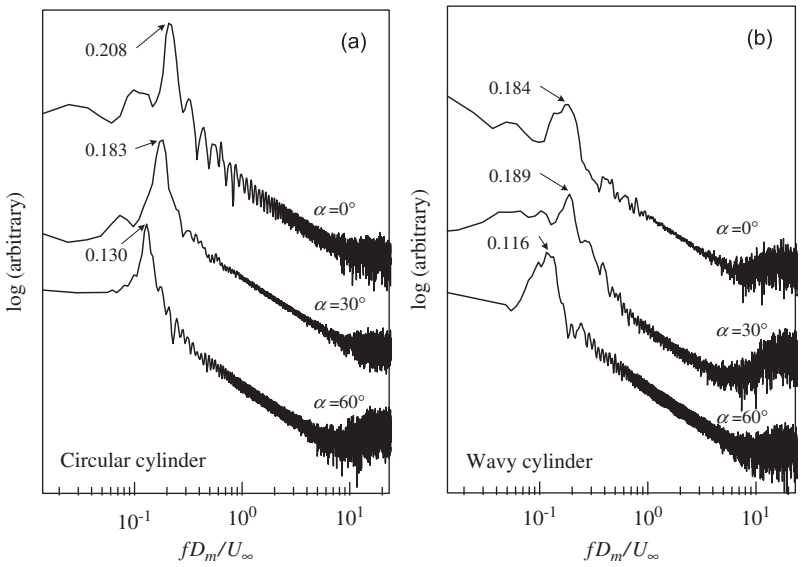

Fig. 15. Strouhal numbers and the power spectra of the lift coefficients of circular or wavy cylinders at Re = 3900. The vertical (logarithmic) scale of the graph is arbitrary, but the same scale is used for each spectrum.

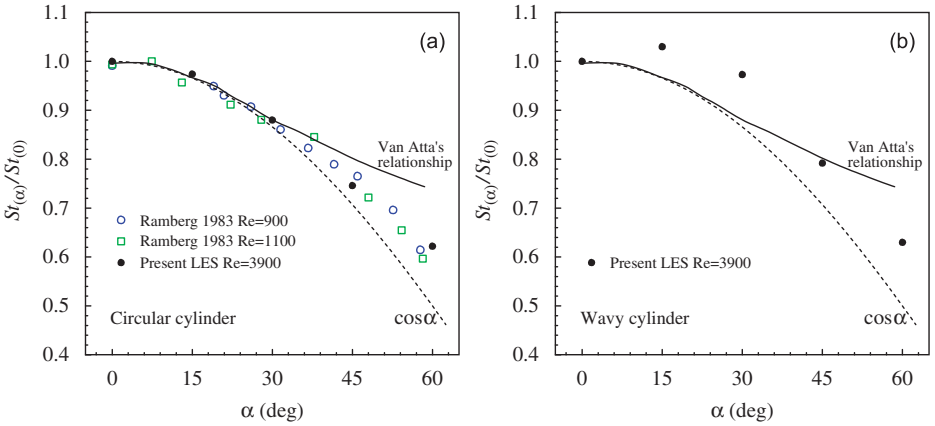

Fig. 16. The ratio of Strouhal numbers for yawed circular cylinders or wavy cylinders.

Fig. 16 further confirms the results illustrated in Fig. 14. The present LES results on $St_{(\alpha)}/St_{(0)}$ for the yawed circular cylinder are close to those obtained by Ramberg (1983) and slightly different from the solid line by Van Atta (1968) for large yaw angles (Fig. 16(a)). The values are also close to the dashed line of the cosine-law distributions for yaw angles $\alpha \leq 45^\circ$. The results show that the Strouhal number on vortex shedding frequency variation with yaw angle does not follow the Independence Principle for yaw angles beyond 45°. Different from that of yawed circular cylinders, the Strouhal number for the yawed wavy cylinder does not obey the Independence Principle in such a subcritical Reynolds number range (Fig. 16(b)).

6. Conclusions

The present study investigates the flow past a yawed wavy cylinder ($\lambda/D_m = 6$, $a/D_m = 0.15$) at a subcritical Reynolds number of 3900 using large eddy simulation (LES). Five different yaw angle conditions are studied. Experimental measurements using the LDA and load cell technique were also carried out to supplement and validate the present LES

method. The present LES results on force coefficients and velocity distributions show good agreement with the experimental measurements.

The unyawed wavy cylinders can result in 14% drag reduction and 80% reduction of fluctuating lift coefficients compared with a corresponding circular cylinder within the same subcritical Reynolds number range. For yawed circular cylinders, it was found that the wake vortices approach a quasi-two-dimensional state with yaw angles up to 45°. Significant differences with the quasi-two-dimensional wake structures can be found for a circular cylinder at $\alpha = 60°$. In general, the yawed circular cylinders followed the Independence Principle up to $\alpha = 45°$. For yawed wavy cylinders, the spanwise sinusoidal waved flow separation line has been modified. With a smaller yaw angle of 15°, the wake vortices still show periodic repetition along the spanwise direction like the unyawed case. The periodic vortex structure becomes more and more incoherent with increasing yaw angle, due to the interaction between the enhancing additional oncoming velocity component in the spanwise direction ($U_\infty \sin\alpha$, in the negative z-direction) and the typical spanwise flow for the wavy cylinder from saddle to node. It is found that the Independence Principle is not suitable for the yawed wavy cylinder cases for $\alpha > 15°$. In general, the mean drag coefficients and the fluctuating lift coefficients of a yawed wavy cylinder are less than those of a corresponding circular cylinder at similar flow condition. As the yaw angle increases, the advantageous effect of wavy cylinder on force and vibration control no longer exists. At $\alpha = 60°$, no significant force reduction can be observed on such wavy cylinder. The large yaw angle affects the surface flow separation of the wavy cylinder and hence greatly modifies the flow pattern behind the wavy cylinder. This also implies that the optimal spanwise wavelength λ/D_m on the control body's vibration and drag reduction may no longer be suitable for wavy cylinders at large yaw angles.

Acknowledgement

The authors wish to thank the Research Grants Council of the Hong Kong Special Administrative Region, China, for its support through Grant no. PolyU 5193/07E.

References

Afgan, I., Moulinec, C., Prosser, R., Laurence, D., 2007. Large eddy simulation of turbulent flow for wall mounted cantilever cylinders of aspect ratio 6 and 10. International Journal of Heat and Fluid Flow 28, 561–574.

Alam, M.M., Zhou, Y., 2007. Turbulent wake of an inclined cylinder with water running. Journal of Fluid Mechanics 589, 261–303.

Bearman, P.W., Owen, J.C., 1998. Reduction of bluff-body drag and suppression of vortex shedding by the introduction of wavy separation lines. Journal of Fluids and Structures 12, 123–130.

Breuer, M., 1998. Numerical and modeling influences on large eddy simulations for the flow past a circular cylinder. International Journal of Heat and Fluid Flow 19, 512–521.

Bursnall, W.J., Loftin, L.K.J., 1951. Experimental investigations of the pressure distribution about a yawed circular cylinder in the critical Reynolds number range. National Advisory Committee for Aeronautics, 1–34.

Chen, L., Tu, J.Y., Yeoh, G.H., 2003. Numerical simulation of turbulent wake flows behind two side-by-side cylinders. Journal of Fluids and Structures 18, 387–403.

Choi, H.C., Jeon, W.P., Kim, J.S., 2008. Control of flow over a bluff body. Annual Review of Fluid Mechanics 40, 113–139.

Darekar, R.M., Sherwin, S.J., 2001. Flow past a square-section cylinder with a wavy stagnation face. Journal of Fluid Mechanics 426, 263–295.

Dobre, A., Hangan, H., Vickery, B.J., 2006. Wake control based on spanwise sinusoidal perturbations. AIAA Journal 44, 485–492.

Drikakis, D., 2003. Advances in turbulent flow computations using high-resolution methods. Progress in Aerospace Sciences 39, 405–424.

Drikakis, D., Hahn, M., Mosedale, A., Thornber, B., 2009. Large eddy simulation using high-resolution and high-order methods. Philosophical Transactions of the Royal Society A 367, 2985–2997.

Franke, J., Frank, W., 2002. Large eddy simulation of the flow past a circular cylinder at $Re_D = 3900$. Journal of Wind Engineering and Industrial Aerodynamics 90, 1191–1206.

Hahn, M., Drikakis, D., 2009a. Assessment of large-eddy simulation of internal separated flow. Journal of Fluids Engineering 131 071201-1-15.

Hahn, M., Drikakis, D., 2009b. Implicit large-eddy simulation of swept-wing flow using high-resolution methods. AIAA Journal 47, 618–630.

Hanson, A.R., 1966. Vortex shedding from yawed cylinders. AIAA Journal 4, 738–740.

Hayashi, T., Kawamura, T., 1995. Non-uniformity in a flow around a yawed circular cylinder. Flow Measurement and Instrumentation 6, 33–39.

Kaneko, S., Kawamura, T., 2002. Numerical study of flow around two yawed and parallel circular cylinders. Theoretical and Applied Mechanics Japan 51, 199–205.
Kawamura, T., Hayashi, T., 1994. Computation of flow around a yawed circular cylinder. JSME International Journal 37, 229–236.
Kozakiewicz, A., Fredsøe, J., Sumer, B.M., 1995. Forces on pipelines in oblique attack: steady current and waves. In: Proceedings of the 5th International Offshore and Polar Engineering Conference, Hague, Netherlands, vol. 2, pp. 174–183.
Kravchenko, A.G., Moin, P., 2000. Numerical studies of flow over a circular cylinder at $Re_D = 3900$. Physics of Fluids 12, 403–417.
Lam, K., Wang, F.H., Li, J.Y., So, R.M.C., 2004. Experimental investigation of the mean and fluctuating forces of wavy (varicose) cylinders in a cross-flow. Journal of Fluids and Structures 19, 321–334.
Lam, K., Lin, Y.F., 2007. Drag force control of flow over wavy cylinders at low Reynolds number. Journal of Mechanical Science and Technology 21, 1331–1337.
Lam, K., Lin, Y.F., 2008. Large eddy simulation of flow around wavy cylinders at a subcritical Reynolds number. International Journal of Heat and Fluid Flow 29, 1071–1088.
Lam, K., Lin, Y.F., 2009. Effects of wavelength and amplitude of a wavy cylinder in cross-flow at low Reynolds numbers. Journal of Fluid Mechanics 620, 195–220.
Lam, K., Lin, Y.F., Zou, L., Liu, Y., 2010. Experimental study and large eddy simulation of turbulent flow around tube bundles composed of wavy and circular cylinders. International Journal of Heat and Fluid Flow 31, 32–44.
Liang, C., Papadakis, G., 2007. Large eddy simulation of pulsating flow over a circular cylinder at subcritical Reynolds number. Computers & Fluids 36, 299–312.
Lilly, D.K., 1966. On the application of the eddy viscosity concept in the inertial subrange of turbulence. NCAR Manuscript, 123.
Lourenco, L., Shih, C., Krothapalli, A., 1992. Observations on the near wake of a yawed circular cylinder. In: Proceedings of the Sixth International Symposium Lisbon, Portugal, pp. 257–284.
Lubcke, H., Schmidt, St., Rung, T., Thiele, F., 2001. Comparison of LES and RANS in bluff-body flows. Journal of Wind Engineering and Industrial Aerodynamics 89, 1471–1485.
Lucor, D., Karniadakis, G.E., 2003. Effects of oblique inflow in vortex-induced vibrations. Flow, Turbulence, and Combustion 71, 375–389.
Ma, X., Karamanos, G.S., Karniadakis, G.E., 2000. Dynamics and low-dimensionality of a turbulent near wake. Journal of Fluid Mechanics 410, 29–65.
Marshall, J.S., 2003. Wake dynamics of a yawed cylinder. Journal of Fluids Engineering 125, 97–103.
Norberg, C., 1987. In: Effects of Reynolds Number and a Low-intensity Freestream Turbulence on the Flow around a Circular Cylinder, Publ. 87/2. Department of Applied Thermodynamics and Fluid Mechanics, Chalmers University of Technology.
Norberg, C., 2001. Flow around a circular cylinder: aspects of fluctuating lift. Journal of Fluids and Structures 15, 459–469.
Pope, S.B., 2004. Ten questions concerning the large-eddy simulation of turbulent flows. New Journal of Physics 6, 1–24.
Ramberg, S.E., 1983. The effects of yaw and finite length upon the vortex wakes of stationary and vibrating circular cylinders. Journal of Fluid Mechanics 128, 81–107.
Shirakashi, M., Ueno, S., Ishida, Y., Wakiya, S., 1984. Vortex excited oscillation of a circular cylinder in a uniform flow. Bulletin of JSME 27, 1120–1126.
Smagorinsky, J., 1963. General circulation experiments with the primitive equations. I. The basic experiment, Monthly Weather Review 91, 99–164.
Thakur, A., Liu, X., Marshall, J.S., 2004. Wake flow of single and multiple yawed cylinders. ASME Journal of Fluids Engineering 126, 861–870.
Tombazis, B., Bearman, P.W., 1997. A study of three-dimensional aspects of vortex shedding from a bluff body with a mild geometric disturbance. Journal of Fluid Mechanics 330, 85–112.
Vakil, A., Green, S.I., 2009. Drag and lift coefficients of inclined finite circular cylinders at moderate Reynolds numbers. Computers & Fluids 38, 1771–1781.
Van Atta, C.W., 1968. Experiments in vortex shedding from yawed circular cylinders. AIAA Journal 6, 931–933.
Williamson, C.H.K., 1996. Vortex dynamics in the cylinder wake. Annual Review of Fluid Mechanics 28, 477–539.
Yeo, D.H., Jones, N.P., 2008. Investigation on 3-D characteristics of flow around a yawed and inclined circular cylinder. Journal of Wind Engineering and Industrial Aerodynamics 96, 1947–1960.
Zdravkovich, M.M, 2003. Flow Around Circular Cylinders. Applications, vol. 2. Oxford University Press.
Zhao, M., Cheng, L., Zhou, T.M., 2009. Direct numerical simulation of three-dimensional flow past a yawed circular cylinder of infinite length. Journal of Fluids and Strucutres 25, 831–847.